



Equilibrium models for lower bound limit analyses of reinforced concrete slabs

E.A.W. Maunder*, A.C.A. Ramsay

Ramsay Maunder Associates, Trehill House, Kenn, Devon, EX6 7XJ, UK

ARTICLE INFO

Article history:

Received 7 January 2011

Accepted 13 February 2012

Available online 10 March 2012

Keywords:

Limit analyses

Hyperstatic

Equilibrium

Concrete slabs

ABSTRACT

The paper addresses lower bound limit analyses of reinforced concrete slabs. The assessment problem is formulated in terms of static variables representing hyperstatic fields of moment, and constraints based on biconic yield criteria. These fields are generated directly within triangular Kirchhoff and Reissner–Mindlin type elements, are highly localised, and lead to very sparse matrices for optimisation programmes. Methods of forming particular equilibrating solutions are presented, which include those recovered from a yield line solution based on the same mesh of elements. Numerical examples are presented with Kirchhoff type elements, including the benchmark problem of a square plate with fixed supports.

© 2012 Civil-Comp Ltd. and Elsevier Ltd. All rights reserved.

1. Introduction

Lower bound limit analysis exploits the plasticity theorem that has been expressed by Heyman as the “master safe theorem” [1]. Hillerborg [2] was an early proponent of lower bound limit analysis for reinforced concrete slabs in the form of the strip method in the days when manual solutions were prominent, and he noted later [3] that computational implementation of such methods had not so far been developed. In the context of the design or assessment of reinforced concrete slabs, the key aspects are the use of statically admissible fields of stress-resultants in equilibrium models, appropriate strength or yield criteria, and an optimisation procedure.

Computational methods for limit analysis for lower bounds have been proposed based on mathematical programming techniques, e.g. linear programming (LP) and second order cone programming (SOCP). Equilibrium has been enforced in a variety of ways, either *a priori* or as linear constraints. However, the enforcement of equilibrium has not always been strictly satisfied, and hence can raise uncertainty as to the safety of the result. Such methods are briefly discussed and referenced in the next paragraph.

An appropriate equilibrium model for slabs depends on whether the yield criterion involves only moments, or involves both moments and shear forces. In the former case use can be made of equilibrium in the Kirchhoff sense, i.e. torsional moments at boundaries or interfaces are replaced by equivalent shear and nodal forces. Computational methods that have been proposed range from modified strip methods based on orthogonal or oblique families of strips [4,5], to exploiting conventional linear elastic finite element models with fictitious plastic strains [6], to limit

analyses based on triangular Kirchhoff elements and equilibrium enforced by linear constraints or by *a priori* processing a global equilibrium matrix, using pivoting, to determine hyperstatic fields [7–10], and to limit analyses based on meshless methods [11,12].

In the case when shear forces are significant and should be involved in the yield criteria, complete equilibrium is required with, in general, continuity of normal bending and torsional moments and normal components of shear force. This situation would normally arise in the case of flat slabs. The stronger sense of equilibrium is accounted for in Reissner–Mindlin plate theory. In both cases we wish to take advantage of a minimum number of static variables in a lower bound limit analysis, as advocated in [7]. However, rather than involve numerical processing of a global equilibrium matrix, we propose a simple direct method to construct independent hyperstatic fields of stress-resultants to be used as static variables. A common yield criterion for moments leads to the biconic yield surface as defined by Nielsen [13] in terms of the top and bottom layers of reinforcement. More refined criteria have been proposed by May and Lodi [14], for moderate levels of reinforcement, which involves a more complicated sandwich model of a slab. The incorporation of transverse shear has also been proposed by Marti [15]. In this paper we will restrict ourselves to the simpler, but common case, of low levels of orthogonal reinforcement when shear failure is unlikely.

The structure of the paper is as follows: Section 2 develops the concepts of directly using moment fields that are *a priori* statically admissible (SAMF), and the formulation of the optimisation problem as a standard second order cone programme (SOCP). The concepts are illustrated with reference to a simple slab in Section 2, and generalised within a finite element framework in Section 3. Section 3 describes triangular equilibrium elements and the construction of independent hyperstatic moment fields in the

* Corresponding author.

E-mail address: E.A.W.Maunder@exeter.ac.uk (E.A.W. Maunder).

context of Kirchhoff and Reissner–Mindlin plate theories. Section 4 considers the formation of particular SAMF in relation to the applied loads. As particular solutions for the optimisation programmes, these may be formed directly from an initial elastic analysis of an equilibrium model, or may be recovered from a similar analysis based on displacement elements, or from a yield line analysis based on rigid triangular elements. Numerical examples are presented in Section 5, and the paper concludes in Section 6 together with directions for future work.

2. Development of concepts via a simple example

This example is based on a particular SAMF defined by Nielsen [13]. A rectangular slab is simply supported on two adjacent sides at $x = -a$ and at $y = -b$, and loaded with a uniform line load on side at $x = a$, as indicated in Fig. 1. The particular moment field \mathbf{m}_0 and two hyperstatic fields \mathbf{m}_1 and \mathbf{m}_2 are defined in Eq. (1),

$$\begin{aligned} \{\mathbf{m}_0\} &= \frac{1}{2} \begin{Bmatrix} a(1 - (\frac{x}{a})^2) \\ 0 \\ b(1 - \frac{x}{a})(1 - \frac{y}{b}) \end{Bmatrix}; \quad \{\mathbf{m}_1\} = \begin{Bmatrix} 1 - (\frac{x}{a})^2 \\ 0 \\ \frac{x}{a^2}(-b + y) \end{Bmatrix}; \quad \text{and} \\ \{\mathbf{m}_2\} &= \begin{Bmatrix} 0 \\ 1 - (\frac{y}{b})^2 \\ \frac{y}{b^2}(-a + x) \end{Bmatrix}. \end{aligned} \quad (1)$$

After torsional moments acting on the sides of the slab are replaced by equivalent Kirchhoff shear forces, the reactions are as defined in Fig. 2.

The second two fields only involve self-balancing distributions of shear and corner forces as reactions, and are thus hyperstatic. These are used to modify the particular solution within an optimisation procedure. As an orthotropic slab, the biconic yield surface, as illustrated in Fig. 3, corresponds to the two yield constraints in Eq. (2) for each constraint point i ,

$$(m_{ix}^h - m_{ix}) \cdot (m_{iy}^h - m_{iy}) \geq m_{ixy}^2, \quad (m_{ix}^s + m_{ix}) \cdot (m_{iy}^s + m_{iy}) \geq m_{ixy}^2, \quad (2)$$

where (m_x^h, m_y^h) and (m_x^s, m_y^s) denote hogging and sagging yield moments due to top and bottom layers of reinforcement in the x and y directions respectively [13].

Constraint points may be dispersed over the domain of the slab in any appropriate manner, but a regular grid of nine points will be used in this example, as indicated in Fig. 1. The components of the moment field in Eq. (2) are linearly related to the load factor λ and the hyperstatic variables in vector $\{\mathbf{X}\}$ in Eq. (3).

$\mathbf{m}^i = \lambda \mathbf{m}_0^i + [\mathbf{B}^i] \cdot \{\mathbf{X}\}$ at point i for $i = 1$ to N , or collectively for all points:

$$\mathbf{m} = \lambda \mathbf{m}_0 + [\mathbf{B}] \cdot \{\mathbf{X}\}. \quad (3)$$

In Eq. (3) suffix 0 denotes particular values of moments that equilibrate with the loads, and matrices $[\mathbf{B}^i]$ contain hyperstatic values of

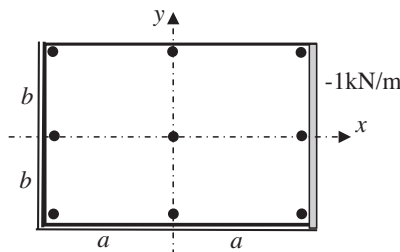


Fig. 1. Rectangular slab with a local coordinate system, and a set of constraint points.

moments at points i . In the case of structural assessment, where the yield moments (m_x^h, m_y^h) and (m_x^s, m_y^s) are already known, the optimisation problem can be expressed as a standard second order cone programme [16] as follows:

Maximise λ subject to:

Equality constraints $\mathbf{m} = \lambda \mathbf{m}_0 + [\mathbf{B}]\{\mathbf{X}\}$, and

Inequality constraints $Z_3^i \geq \sqrt{(Z_1^i)^2 + (Z_2^i)^2}$ for $i = 1, \dots, N$, where

$$\{\mathbf{Z}^i\} = \begin{cases} 0.5((m_x^i - m_y^i) - (m_x^{ih} - m_y^{ih})) \\ m_{xy}^i \\ 0.5(-(m_x^i + m_y^i) + (m_x^{ih} + m_y^{ih})) \end{cases} \quad \text{or} \quad \begin{cases} 0.5((m_x^i - m_y^i) + (m_x^{is} - m_y^{is})) \\ m_{xy}^i \\ 0.5((m_x^i + m_y^i) + (m_x^{is} + m_y^{is})) \end{cases} \quad (4)$$

for the hogging or sagging cones respectively.

The inequality constraints in Eq. (4) are derived from those in Eq. (2) by moving the apexes of the cones to the origin of a Cartesian axis system (Z_1, Z_2, Z_3) .

A typical inequality constraint can then be visualised in terms of the Lorentz cone in Fig. 4 defined by $Z_3 = r = \sqrt{Z_1^2 + Z_2^2}$. A constraint becomes $Z_3 \geq r$.

In the case of design, the load factor is known and we can express the yield moments as linear functions of a set of design parameters. Eq. (4) can then be rearranged into a standard form containing hyperstatic and design parameters as variables. The objective function may then be a linear cost function of the design parameters.

3. Finite element implementation using equilibrium elements

Implementation of the procedures outlined in Section 2 can be generalised by exploiting equilibrium elements within a finite element framework. Such elements have been previously formulated as hybrid elements [17–19], and we consider here Kirchhoff or Reissner–Mindlin types of element in their triangular forms. Internal moment fields are assumed to be in polynomial form, and the number of independent fields is given by $(p^2 + 5p + 3)$ where p denotes the degree [19]. In this section we focus on the formation of localised hyperstatic fields of moment and shear. These can be considered in a hierarchical way starting with moment fields of degree 0, as in the Morley element [17], and adding further fields as the degree increases.

3.1. The Kirchhoff type of element

This type of element requires continuity of normal bending moments and equivalent Kirchhoff shear forces across element interfaces, and equilibrium of equivalent nodal forces. The degree of static indeterminacy, α , of a singly connected patch of Kirchhoff elements with static boundary conditions is now established.

Denote the number of elements, edges and nodes in the patch by: m , e , and n respectively. α is given by the number of independent moment fields less the number of independent equilibrium conditions at the edges and nodes. There are $(p + 1)$ conditions for normal edge moments plus p conditions for equivalent Kirchhoff edge shear forces plus 1 condition for each set of nodal forces. Three of these conditions are dependent due to the requirement for overall equilibrium, leading to Eq. (5).

$$\alpha = (p^2 + 5p + 3)m - ((2p + 1)e + n) + 3. \quad (5)$$

The edges and nodes can be classified as internal or external, the latter term signifying that the entities lie on the boundary of the

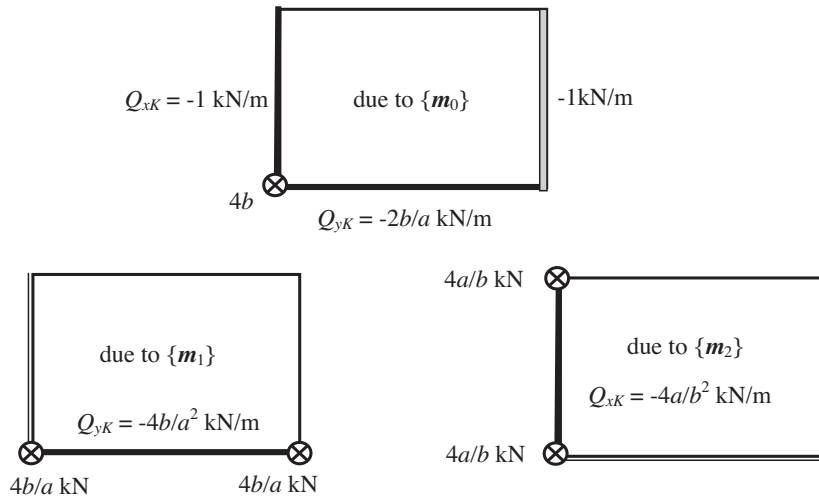


Fig. 2. Equivalent Kirchhoff reactions.

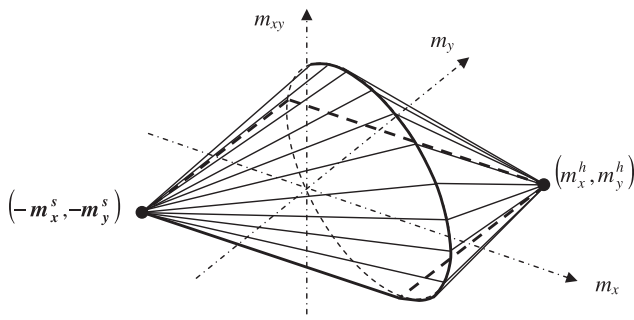


Fig. 3. Biconic yield surface for an orthotropic slab.

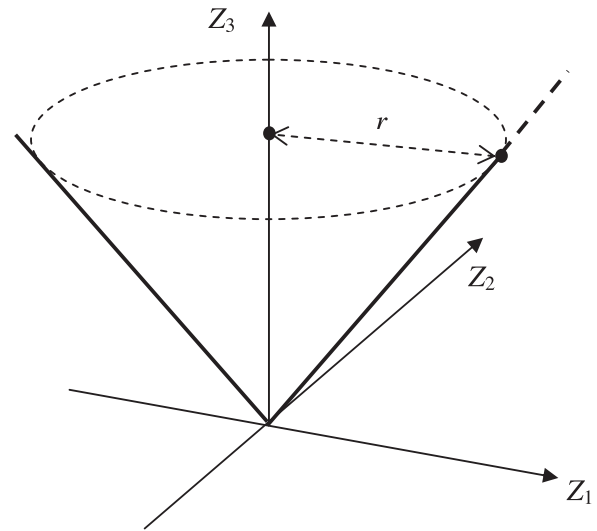


Fig. 4. Alternative Lorentz (ice cream) cones for hogging and sagging cones.

domain. Then $e = e_{int} + e_{ext}$ and $n = n_{int} + n_{ext}$, and because the domain is singly connected:

$$3m = (2e_{int} + e_{ext}) = (3e - 3n + 3) = 3e_{int} + 3e_{ext} - 3n_{int} - 3n_{ext} + 3. \tag{6}$$

Since also $e_{ext} = n_{ext}$ for a boundary that forms a single closed loop, we have the following topological property of the patch:

$$e_{ext} = e_{int} - 3n_{int} + 3. \tag{7}$$

Eq. (5) can now be recast in the general form of Eq. (8).

$$\alpha = m \cdot p(p - 1) \text{ (in type I subdomains)} + e_{int} \cdot 2p \text{ (in type II subdomains)} + n_{int} \cdot 2 \text{ (in type III subdomains)}. \tag{8}$$

The Kirchhoff elements are themselves twice hyperstatic when they have quadratic moment fields, but they are isostatic for linear and constant moment fields. Hence it is possible to define independent hyperstatic fields for a domain within local subdomains of various types, as illustrated in Fig. 5, in a hierarchical way according to the degree of the moment field:

For degree 0, there are two constant fields within each subdomain of type III i.e. a closed star patch of elements with just a single internal node;

For degree 1, there are in addition two linear fields in each subdomain of type II, i.e. a pair of adjacent elements;

For degree 2, there are in addition two quadratic fields in each subdomain of type II and two hyperstatic quadratic fields in each subdomain of type I, i.e. a single element, corresponding to South-

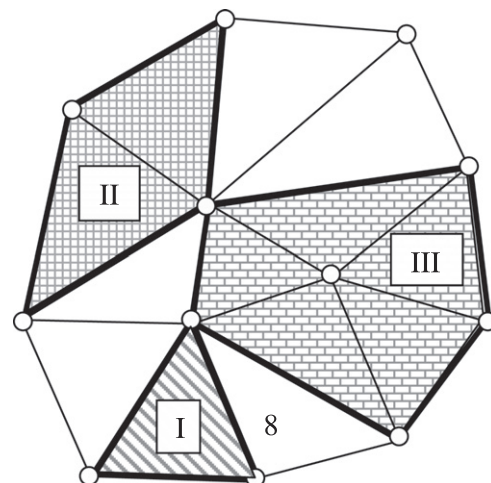


Fig. 5. Singly connected domain (patch) of elements with three types of subdomain.

well functions $U = L_1L_2L_3$ and $V = L_1L_2L_3$, where L_1 , L_2 , and L_3 are the area coordinates.

The transfer of constant moments between adjacent elements in a subdomain of type III is illustrated in Fig. 6, where the arrows at the midpoints of edges indicate resultant moment vectors.

Linear and quadratic moment fields are derived from Southwell stress functions U and V as detailed in Fig. 7. The transfer of moments and equivalent Kirchhoff shear forces between adjacent elements in subdomains of type II is also illustrated in this figure.

The presence of kinematic boundary conditions and/or openings leads to an increase of α , and the set of hyperstatic fields can be extended to form a complete basis using similar forms of construction.

3.2. The Reissner–Mindlin type of element

In this case continuity is enforced at element interfaces between normal bending moments, torsional moments about the normal axis, and the transverse shear force. However restrictions are imposed on these components as element tractions in order to be equilibrated by internal polynomial moment fields of appropriate degree, i.e. in order to be admissible [19,20]. One way to overcome these restrictions is to subdivide the element into three triangular “primitive” elements as first proposed by Sander [21], and such elements will be referred to as macro-elements.

The macro-element with piecewise linear moment fields is isostatic and it can transmit arbitrary linear distributions of moment tractions or constant distributions of shear traction on its sides provided the tractions are in overall equilibrium. This implies that a patch of type III contains three hyperstatic moment fields when side moments and/or side shear forces are constant, and patches of type II contain two further hyperstatic moment fields corresponding to linear distributions of torsional moment along the interfaces.

If we permit quadratic moment fields, then patches of type II contain three further hyperstatic moment fields corresponding to quadratic distributions of moment along the interfaces, and a combination of a linear distribution of shear forces with a counterbalancing constant distribution of torsional moments. Furthermore the quadratic macro-element is itself hyperstatic of degree 6 when considered as a patch of type I. The number of hyperstatic fields for general moment degree p [20] is summarised in Eq. (9), and a similar hierarchic structure to that described for Kirchhoff elements could be organised in order to exploit these fields.

$$\begin{aligned} \alpha = & m \cdot 3p(p-1) \text{ (in type I subdomains)} \\ & + e_{\text{int}} \cdot (3p-1) \text{ (in type II subdomains)} \\ & + n_{\text{int}} \cdot 3 \text{ (in type III subdomains)}. \end{aligned} \quad (9)$$

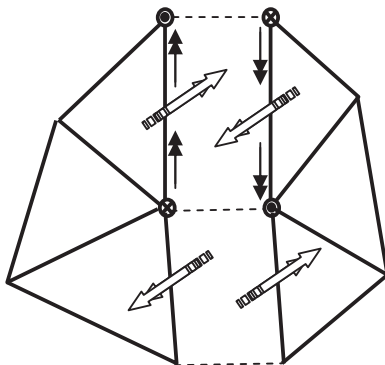


Fig. 6. Transfer of hyperstatic constant moments in a subdomain of type III.

4. Particular solutions

The hyperstatic moment fields serve as the static variables in the optimisation process. However a particular statical solution is required to complete a SAMF. Although the particular solution is arbitrary, we will outline two approaches which are intended to serve as “good” solutions prior to optimisation.

4.1. Particular solutions from a yield line analysis

The first approach involves recovery from a preliminary yield line analysis based on rigid triangular elements that are allowed to yield along interfaces between adjacent elements [22]. This type of analysis generates a weak form of equilibrium which involves constant normal bending moments on the sides of elements and nodal shear forces that represent interaction between elements and distributed loads applied over the area of an element.

As Kirchhoff elements, internal constant moment fields can be uniquely defined to balance the side moments. When loads are uniformly distributed, additional quadratic fields of moment can also be defined to complete the equilibrium of a particular solution [18]. This definition is based on a system of 3-way spanning beam strips which are simply supported on the sides of an element so as to lead to uniform shear reactions around its boundary. However, if the mesh is sufficiently refined, then equilibrium defaults resulting from neglecting these additional fields may be insignificant.

Alternatively, a strong form of equilibrium in Reissner–Mindlin type elements can be recovered by first splitting the nodal forces and replacing them by codiffusive statically equivalent distributions of constant shear force and torsional moment acting on the sides of an element, as indicated in Fig. 8 [23]. Piecewise linear moment fields can then be uniquely determined within each macro-element to be statically admissible with the constant modes of distribution of side tractions. In the event that a uniformly distributed load is applied over the element, the moment field is extended to account for the load in the same way as in the preceding paragraph.

The main advantage of this approach is that it enables both upper and lower bound solutions to be derived from the same mesh of finite elements, and without requiring a linear elastic solution.

4.2. Particular solutions from a linear elastic analysis

In this approach SAMF are either obtained directly from a finite element analysis based on triangular hybrid equilibrium elements [19], or are recovered from a finite element analysis based on more conventional displacement type elements that include nodal shear forces and moments (e.g. Reissner–Mindlin elements based on standard shape functions for the interpolation of deflections and rotations). In the latter case, splitting or resolution of nodal forces and moments is carried out, in a similar way as described in Section 4.1, to produce statically equivalent codiffusive distributions of side tractions [24]. SAMF are then determined for an element by solving a local linear elastic problem. Alternative techniques for recovering SAMF, which are approximately compatible, in a complete finite element model are also being investigated for plates using partition of unity concepts [25].

The advantage of carrying out an initial linear elastic analysis is that, although the results of an analysis are somewhat dependent on the type of element and the mesh used, moment redistribution, using hyperstatic fields in the context of limit analysis, could then be controlled so as to limit the changes in moments. This may be required for reinforced concrete slabs when questions of ductility arise [26]. It is worth noting here that EC2 [26] emphasises that

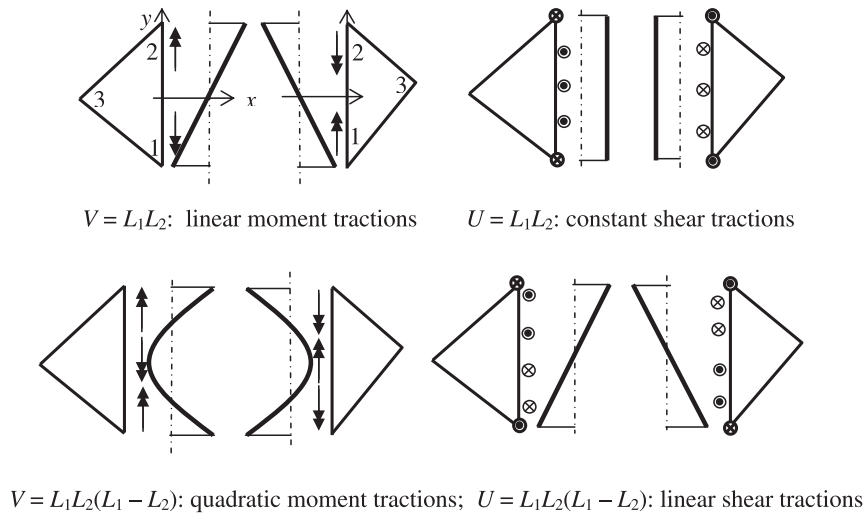


Fig. 7. Hyperstatic element interactions in subdomains of type II.

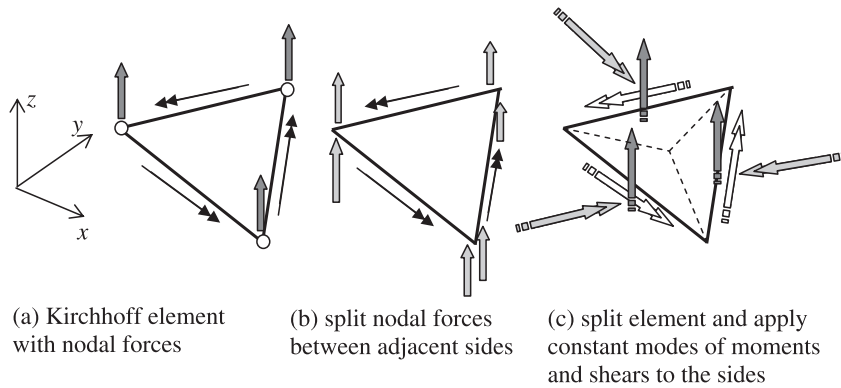


Fig. 8. Transformation from Kirchhoff type element to a Reissner–Mindlin type macro-element.

“The moments at ULS calculated using a linear elastic analysis may be redistributed, provided that the resulting distribution of moments remains in equilibrium with the applied loads”.

5. Numerical examples

5.1. Example in Section 2

As a numerical example of an assessment problem, without recourse to a finite element model of triangular elements, consider the slab in Fig. 1 when $a = b = 1$. Let the slab be homogeneous and isotropic, with equal magnitudes of hogging and sagging yield moments, i.e. let $m^h = m^s = m^Y$. With reference to Fig. 4, Eqs. (3) and (4) simplify for point i with coordinates (x^i, y^i) to Eq. (10).

$$\{m^i\} = \frac{\lambda}{2} \begin{Bmatrix} (1 - (x^i)^2) \\ 0 \\ (1 - x^i) \cdot (1 - y^i) \end{Bmatrix} + \begin{bmatrix} (1 - (x^i)^2) & 0 \\ 0 & (1 - (y^i)^2) \\ x^i(y^i - 1) & y^i(x^i - 1) \end{bmatrix} \begin{Bmatrix} X_1 \\ X_2 \end{Bmatrix},$$

and

$$\{Z^i\} = \begin{Bmatrix} 0.5((m_x^i - m_y^i)) \\ m_{xy}^i \\ 0.5(-(m_x^i + m_y^i) + 2m^Y) \end{Bmatrix} \text{ or } \begin{Bmatrix} 0.5((m_x^i - m_y^i)) \\ m_{xy}^i \\ 0.5((m_x^i + m_y^i) + 2m^Y) \end{Bmatrix}. \tag{10}$$

We could now solve the inverse design problem, i.e. find the minimum value of m^Y for a unit value of λ . For any value of the vector $\{X\}$, it is now an easy matter to determine the maximum value of m^Y that satisfies all the cone constraints. Then $\{X\}$ can be varied in order to determine the minimum of the maximum values of m^Y , and this results in $m^Y = 0.773$ kNm/m at critical constraint points 2, 5, and 8 in Fig. 9, when $[X] = [-0.386 - 0.286]$. Since we now have the optimum relation between m^Y and λ , we can use the inverse of

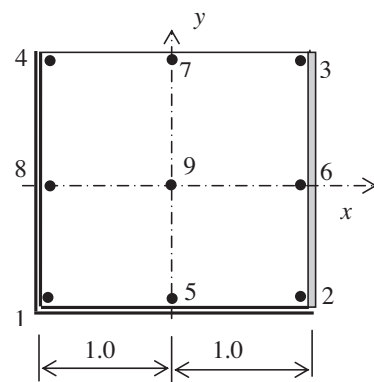


Fig. 9. Location of constraint points for the square plate problem.

this relation to conclude that, if $m^Y = 1$, then $\lambda = 1.2937$. This result has also been confirmed using the version of SOCP as implemented by MOSEK optimisation software [27].

However, the pattern of constraint points may overlook more critical intermediate points, and this is checked by scanning the whole domain with X as already found.

The scan reveals that yield is violated most at a point located at $(0.5, -1.0)$ where the yield utilisation ratio (YUR) becomes 1.019 due to a hogging moment. This ratio is defined by the length of the moment vector in (m_x, m_y, m_{xy}) space divided by the length of the vector when projected onto the yield surface. Fig. 10 illustrates the variation of YUR over five sections where x is constant, including the section at $x = 0.5$ where the ratio is greatest. The implication is that this solution gives a safe lower bound with $m^Y = 1$ if it is scaled, and then λ is reduced to $1.2937/1.019 = 1.270$.

A good quality reference solution is derived for comparison using similar concepts in a finite element model. Using SOCP and a regular finite element mesh, with 3600 elements based on linear hyperstatic moment fields and using seven constraint points per element, the lower bound achieved is given by $\lambda = 1.581$. The corresponding variation of the yield utilisation ratio is plotted as a surface in Fig. 11.

5.2. A benchmark problem: isotropic square slab with fixed sides

Another example employing finite elements concerns the problem of a homogeneous isotropic square plate with fixed sides of

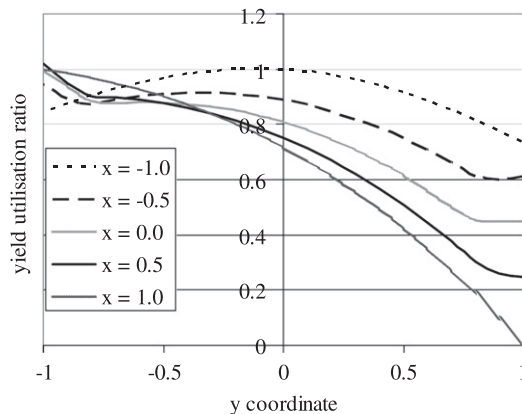


Fig. 10. Sections through the YUR surface based on the two hyperstatic variables.

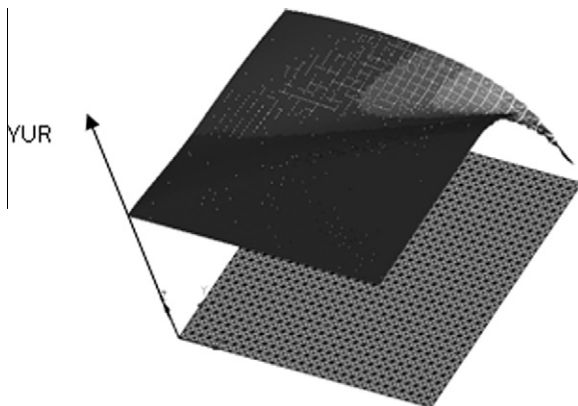


Fig. 11. Surface plot of yield utilisation ratio for a regular mesh with 3600 triangular elements. Dark surface indicates $YUR \rightarrow 1.0$, light surface indicates $YUR \rightarrow 0.0$.

unit length, subject to a UDL and constrained by the Nielsen yield criterion with $m^Y = 1$. This problem serves as a useful benchmark problem since it is one of the few for which an analytical greatest lower bound solution is known [28], i.e. the maximum load factor $\lambda = 42.851$.

Particular solutions are based on yield line analyses for regular meshes up to 256 elements. The corresponding yield line patterns are shown in Fig. 12. The equilibrium solutions are derived from linear, $p = 1$, and quadratic, $p = 2$, Kirchhoff elements with the quadratic moment field constructed as explained in Section 4.1 serving as the particular solution for the uniformly distributed load.

Optimisation was carried out for both upper and lower bound solutions using LP with the interior point method and SOCP respectively. A comparative lower bound solution was also obtained by using a faceted yield surface, with eight facets inscribed within the two cones, to approximate the biconic yield surface in a way to simulate the Wood-Armer equations [29,30]. For this solution, a LP was again used for optimisation, and the error in λ was 6% on the conservative side with a mesh of some 500 elements.

The best lower bound solution in Fig. 12 is based on 32 linear elements for the whole plate, and gives $\lambda \approx 42.0$. The results for lower bound load factors can be compared with recent results obtained by Krabbenhoft et al. [31] of 42.820 based on a regular mesh of 2500 linear elements modelling one-eighth of the plate, Krabbenhoft et al. [32] of 42.831 based on a regular mesh of 8192 elements modelling one-quarter of the plate using SOCP, and Le et al. [12] of 42.83 based on a regular 40×40 grid of nodes for the whole plate and an element free Galerkin method.

5.3. Moment redistribution associated with concentrated loads or supports

The final two examples concern redistribution of moments in the vicinity of a concentrated load or a column support, in the context of a reinforced concrete flat slab. In these examples an elastic field of moments is derived based on Reissner–Mindlin theory with equilibrium elements, assuming uncracked plain concrete with $E = 25$ GPa and $\nu = 0.2$, and then full plastic redistribution is accounted for based on Kirchhoff elements and orthotropic reinforcement with equal yield moments for hogging and sagging.

5.3.1. Concentrated load

This example concerns a $12 \text{ m} \times 6 \text{ m}$ rectangular slab of thickness 0.2 m, simply supported on the longer edges and free on the shorter edges. The load consists of 100 kN as a UDL over a central square area of side length 0.2 m. The yield moment in the span direction is 100 kNm/m, whilst that in the transverse direction is $\mu \times 100$ kNm/m where $\mu \leq 1$. Advantage is taken of symmetry, and the results are shown for a quadrant with the load applied at the origin. Figs. 13–15 present surface plots, with contours, of components of moment, where positive components are plotted above the mesh and negative components are plotted below the translucent mesh.

The relatively high elastic moments in the neighbourhood of the load are redistributed in the isotropic and the anisotropic cases such that an effective width of slab fully exploiting the m_y capacity can be identified in Figs. 16 and 17. At midspan, this width closely corresponds to the position of the hogging yield line and to the total width of the yield zones indicated in these figures. The yield line pattern indicated in Fig. 16 was optimised in each case using a single geometric variable: the horizontal distance of the hogging yield line from the centre.

The surface plots of the components of moment exhibit waves of “creasing” and “tearing” at element interfaces in the vicinity of the sagging yield line after redistribution, whilst fully satisfying local equilibrium within elements. These features may be partly

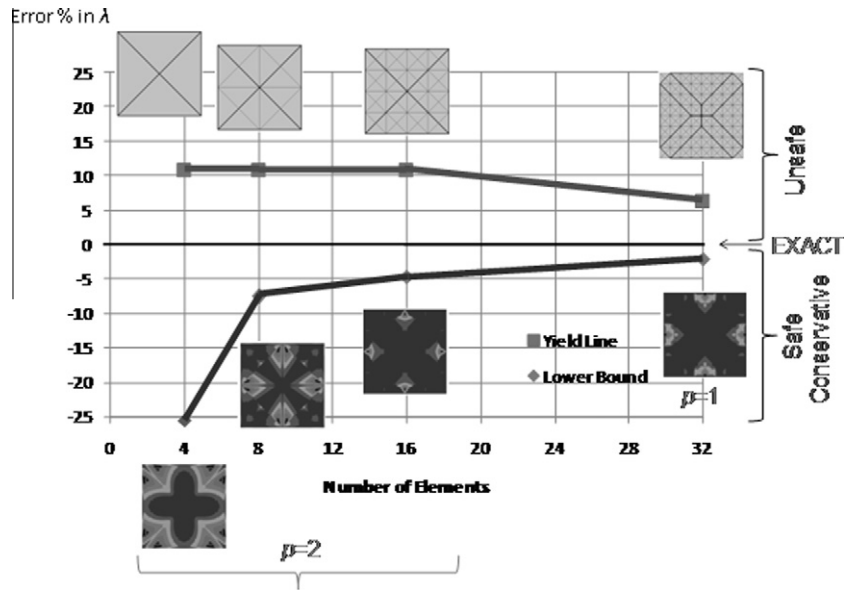


Fig. 12. Convergence of limit analyses with number of elements. The lower bound solutions are presented in terms of YUR grey scale contours, where black indicates $YUR \approx 1.0$, and white indicates $YUR \approx 0.0$.

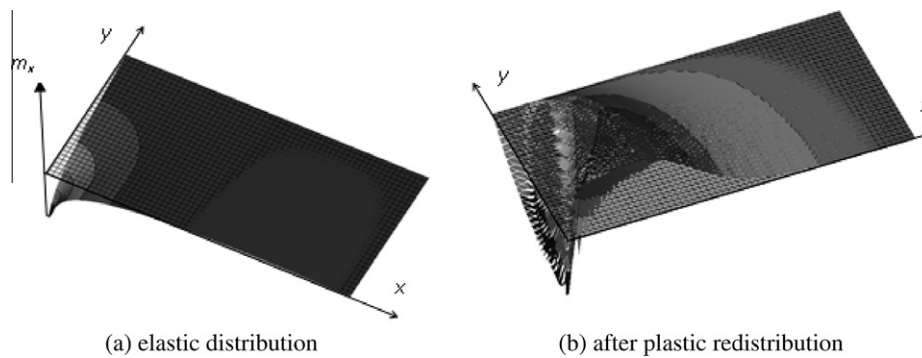


Fig. 13. Surface plots with contours of m_x when $\mu = 0.1$.

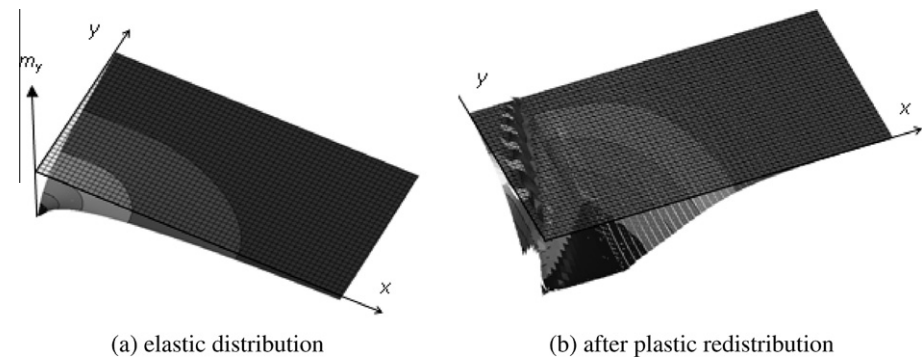


Fig. 14. Surface plots with contours of m_y when $\mu = 0.1$.

attributable to the presence of large moment gradients produced by the anisotropy in a regular but biased mesh of Kirchhoff elements, for which only the normal bending moment is required to be continuous at the interfaces. Another contributory factor may be the potential for non-unique solutions for moments in the vicinity of the sagging yield line. Here the moment contours in Figs. 13–15 indicate that the torsional moment predominates, which implies that yielding is occurring in the neighbourhood of the intersection of the two cones of the biconic yield surface.

5.3.2. Concentrated supports

This example simulates a square flat slab with a uniformly distributed load supported on a symmetric arrangement of four blade columns of length 0.5 m, as indicated in Fig. 18. The centre of the column on line OA is situated at the midpoint of this line.

The slab is assumed to have equal isotropic moment capacities for both hogging and sagging moments. After plastic redistribution, the zones of slab that are at full yield are indicated for the complete slab by the shaded areas, and in the surface plot of YUR for the one

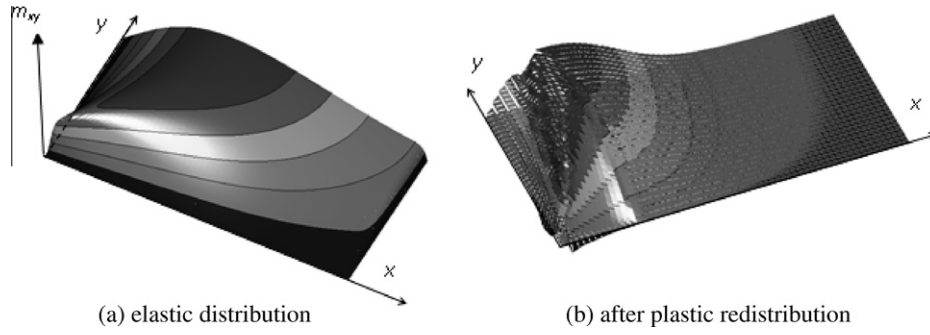


Fig. 15. Surface plots with contours of m_{xy} when $\mu = 0.1$.

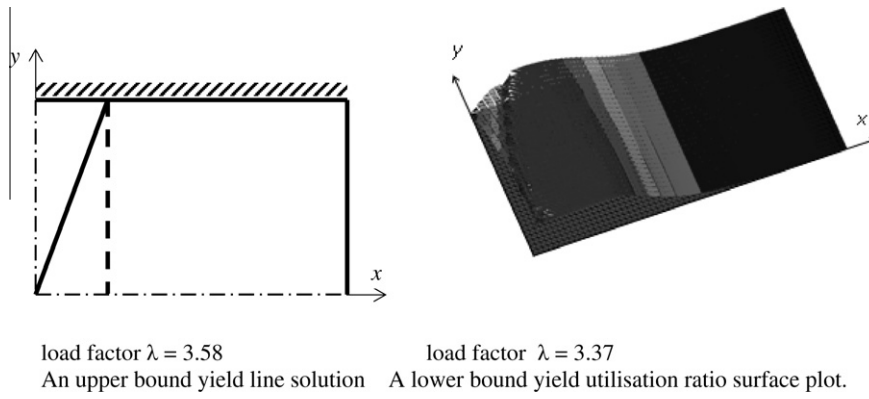


Fig. 16. Upper and lower bound solutions with $\mu = 0.1$.

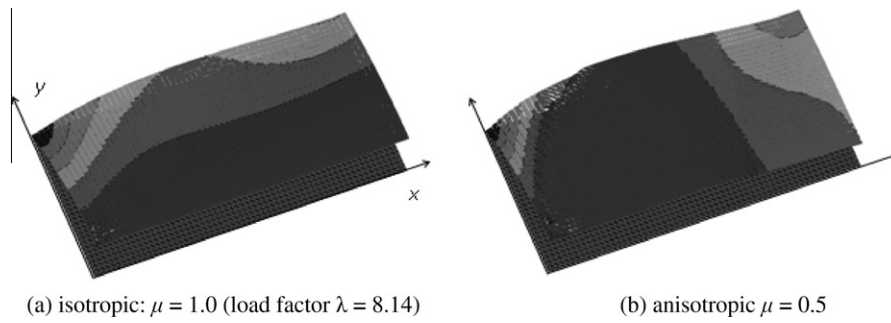


Fig. 17. Lower bound yield utilisation ratio surface plots. Dark surface indicates $YUR \rightarrow 1.0$, light surface indicates $YUR \rightarrow 0.0$.

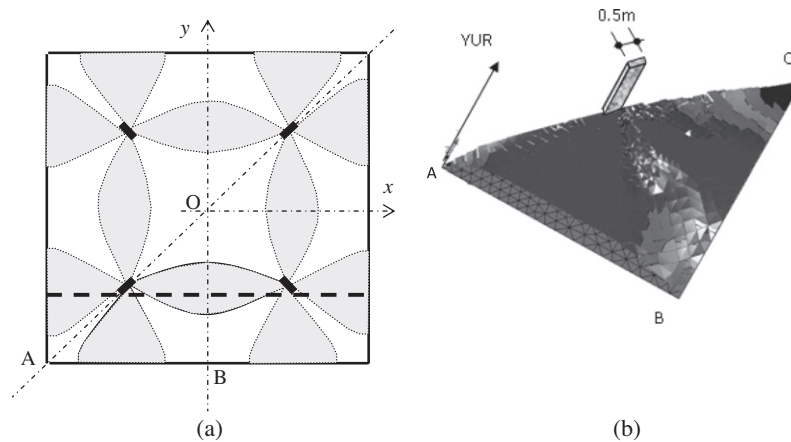


Fig. 18. (a) Isotropic flat slab: grey zones indicate full yield, dashed line indicates a possible hogging yield line and (b) yield utilisation ratio surface plot for area OAB.

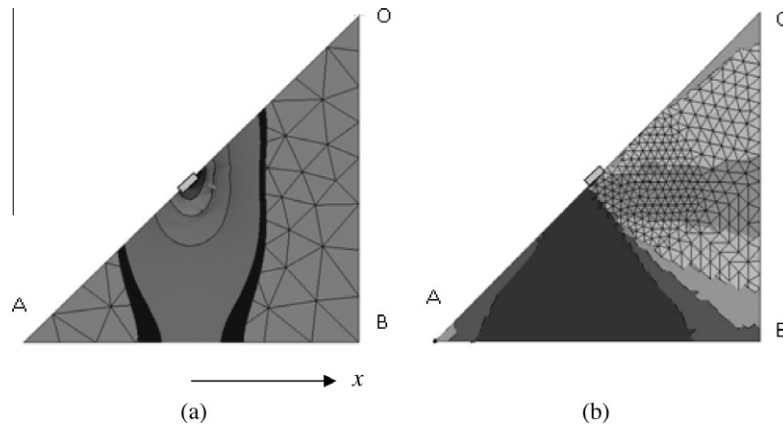


Fig. 19. m_x Moment fields: (a) elastic, and (b) fully redistributed plastic. Sagging moments occur where the finite element mesh is visible.

eighth area OAB in Fig. 18. The distributions of the component of moment m_x are shown qualitatively in Fig. 19 for the elastic and fully redistributed plastic moments after scaling so as to equilibrate with a unit pressure load. Then the ranges of principal moments are:

- 1.73 to 10.60 kNm/m for elastic moments, and
- 4.0 to 4.0 kNm/m for plastic moments.

These imply that if the slab is designed to withstand the distribution of elastic moments as ultimate moments, then the plastic load capacity is factored by $10.60/4.00 = 2.65$ assuming that adequate ductility is available. This may be compared with a yield line solution based on a single hogging yield line, positioned as indicated in Fig. 18, which would give a load factor of $10.6/3.9853 = 2.66$.

This example again illustrates how the relatively high elastic moments that occur at supports can be redistributed into the neighbouring areas to give yield zones as opposed to yield lines, and thereby reduce the design moments in a rational way whilst maintaining equilibrium. Further results of investigations into these examples can be found at the authors' website [33].

6. Conclusions and future directions

A lower bound, and hence safe, method of assessing the load capacity of a reinforced concrete slab has been presented. The method exploits the possibility of direct hierarchical construction of localised hyperstatic fields of stress-resultants for finite element equilibrium models using either Kirchhoff or Reissner–Mindlin types of element. The method leads to highly sparse formulations of linear or second order cone programmes for optimisation.

The use of a similar finite element mesh to initially obtain an upper bound yield line solution enables both types of bound to be realised, and the yield line solution also provides the data for a particular equilibrating field of moments to be determined for use in the lower bound analysis.

Initial results appear to be promising, and future developments will be aimed at:

Investigating the effects of using a set of hyperstatic fields that form an incomplete basis for the complementary solution space;

Investigating the use of other forms of yield criteria for moments, such as von Mises in the context of metallic plates, and the more conservative criteria for reinforced concrete slabs proposed by May et al. [14].

Investigating extensions of yield criteria to include the effects of shear in a sandwich model as proposed by Marti [15] together with appropriate Reissner–Mindlin type elements.

Formulating the slab assessment problem to account for limited ductility by conforming with simplified code requirements that limit moment redistribution from an initial linear elastic solution.

Extending lower bound optimisation in the context of design, where both design and static variables are involved.

Elastic shakedown.

Acknowledgements

Grateful acknowledgements are due to the suppliers of the Mosek software package for their policy which allowed free use of the software during development of current applications by Ramsay Maunder Associates [33].

References

- [1] Heyman J. The establishment of plastic design in the UK. *Proc Inst Civil Engrs Eng History Heritage* 2009;EH1:7–11.
- [2] Hillerborg A. Strip method of design. Viewpoint, Wexham Springs; 1975.
- [3] Hillerborg A. Strip method design handbook. London: E&FN Spon; 1996.
- [4] O'Dwyer DW, O'Brien EJ. Design and analysis of concrete slabs using a modified strip method. *Struct Engr* 1998;76(17):329–33.
- [5] Burgoyne C, Smith A. Automated lower bound analysis of concrete slabs. In: Burgoyne, Lees, Middleton, editors. *Morley symposium on concrete plasticity and its applications*. CUED technical report CUED/D-STRUCT/TR.222, Department of Engineering, University of Cambridge; 2007. p. 49–192.
- [6] Anderheggen E. Finite elements, plasticity theory and linear programming for dimensioning reinforced concrete slabs and walls. In: Roorda, Srivastava, editors. *Trends in structural mechanics*. Dordrecht, The Netherlands: Kluwer Academic Publishers; 1997. p. 225–34.
- [7] Krabbenhoft K, Damkilde L. Lower bound limit analysis of slabs with nonlinear yield criteria. *Comput Struct* 2002;80:2043–57.
- [8] Johnson D. Collapse analysis of reinforced concrete slabs: are the up and down roads one and the same? In: Pandey et al., editors. *Advances in engineering structures mechanics & construction*. Springer; 2006. p. 823–31.
- [9] Le CV, Nguyen-Xuan H, Nguyen-Dang H. Upper and lower bound limit analysis of plates using FEM and second-order cone programming. *Comput Struct* 2010;88:65–73.
- [10] Jackson AM, Middleton CR. Assessing the flexural collapse load of concrete slabs. In: *Poster category of the "IStructE Young Researchers' conference"*. London: Institution of Structural Engineers; March 2009.
- [11] Chen S, Liu Y, Cen Z. Lower bound limit analysis by using the EFG method and non-linear programming. *Int J Numer Methods Eng* 2008;74:391–415.
- [12] Le CV, Gilbert M, Askes H. Limit analysis of plates and slabs using a meshless equilibrium formulation. *Int J Numer Methods Eng* 2010. doi:10.1002/nme.2887.
- [13] Nielsen MP. *Limit analysis and concrete plasticity*. 2nd ed. CRC Press; 1998.
- [14] May IM, Lodi SH. Deficiencies of the normal moment yield criterion for RC slabs. *Proc Inst Civil Engrs Struct Build* 2005;158. p. SB6: 371–80.
- [15] Marti P. Design of concrete slabs for transverse shear. *ACI Struct J* 1990;87(2):180–90.
- [16] Alizadeh F, Goldfarb D. Second-order cone programming. *Math Prog Ser B* 2003;95:3–51.
- [17] Morley LSD. The triangular equilibrium element in the solution of plate bending problems. *Aero Quart* 1968;19:149–69.
- [18] Fraeijs de Veubeke BM, Sander G. An equilibrium model for plate bending. *Int J Solids Struct* 1968;4:447–68.

- [19] Mauger EAW, Moitinho de Almeida JP. A triangular hybrid equilibrium plate element of general degree. *Int J Numer Methods Eng* 2005;63:315–50.
- [20] Mauger EAW, Moitinho de Almeida JP. The stability of stars of triangular equilibrium plate elements. *Int J Numer Methods Eng* 2009;77:922–68.
- [21] Sander G. Application of the dual analysis principle. In: Fraeijs de Veubeke, editor. High speed computing of elastic structures. *Les Congrès et Colloques de l'Université de Liège*, vol. 61; 1971. p. 167–207.
- [22] Munro J, Da Fonseca AMA. Yield line method by finite elements and linear programming. *Struct Engr* 1978;56B(2):37–44.
- [23] Mauger EAW, Ramsay ACA. Limit analysis of slabs revisited with finite element models. In: Abel, Cooke, editors. CD of 6th international conference on computation of shell and spatial structures (IASS-IACM), Ithaca, NY, USA; 2008.
- [24] Ladeveze P, Mauger EAW. A general method for recovering equilibrating element tractions. *Comput Methods Appl Mech Eng* 1996;137:111–51.
- [25] Moitinho de Almeida JP, Mauger EAW. Recovery of equilibrium on star patches using a partition of unity technique. *Int J Numer Methods Eng* 2009;79:1493–516.
- [26] Eurocode 2: Design of concrete structures, Part 1-1: General rules and rules for buildings. EN 1992-1-1, 2004.
- [27] MOSEK optimization software, Mosek ApS, Copenhagen, Denmark. <www.mosek.com>.
- [28] Fox EN. Limit analysis for plates: the exact solution for a clamped square plate of isotropic homogeneous material obeying the square yield criterion and loaded by uniform pressure.. *Philos Trans Roy Soc London Ser A Math Phys Sci* 1974;277(1265):121–55.
- [29] Wood RH. The reinforcement of slabs in accordance with a predetermined field of moments. *Concrete* 1968;2:69–76.
- [30] Armer GST. Correspondence. *Concrete* 1968;2:319–20.
- [31] Krabbenhoft K, Damkilde L. A general non-linear optimization algorithm for lower bound limit analysis. *Int J Numer Methods Eng* 2003;56:165–84.
- [32] Krabbenhoft K, Lyamin AV, Sloan SW. Formulation and solution of some plasticity problems as conic programs. *Int J Solids Struct* 2007;44:1533–49.
- [33] Ramsay Mauger Associates. The Innovation Centre, University of Exeter. <www.ramsay-mauger.co.uk>.